2024 IEEE/ASME International Conference on Advanced Intelligent Mechatronics (AIM)
July 15-19, 2024. Boston, MA, USA

Force, Humidity, and Temperature Estimation of a Multi-modal Soft Actuator for Human-Pad Interface

Pat Twomey, Vaibhavsingh Varma, and Mitja Trkov

***Abstract*— Pressure injuries in long-term care facilities present a significant problem for the well-being of bedridden patients and the overall cost of the healthcare systems. Mitigating risks of pressure injury formation might be possible through monitoring and control of the main extrinsic factors that cause them, including temperature, humidity, and normal and shear loads at the skin-support surface interface. An instrumented soft robotic pad system serving as a support surface is a potential solution. In this work, we present the design of two-degree-of-freedom soft actuators that when combined in a grid form an instrumented soft pad. The actuators have integrated humidity sensor, thermistor, and embedded force sensitive resistor (FSR). We investigate the optimal placement of the embedded sensors to monitor temperature, humidity, and applied normal loads during various actuation modes. We utilize a long short-term memory (LSTM) neural network to obtain estimated values of humidity and temperature at the expected contact interface, and also estimates of the normal loads exerted on the soft actuators under various actuation configurations that affect raw FSR sensor measurements. The developed system can be potentially used to monitor and mitigate pressure injuries risks factors in long-term care patients and enhance the quality of care of those patients.**

I. Introduction

Pressure injuries in long-term care facilities pose a significant challenge for the welfare of bedridden patients. Each year, more than 2.5 million people in the US develop pressure injuries [1]. Increased risks for pressure injuries have been associated with extrinsic factors including temperature, humidity, and both normal and shear loads at the skin-pad interface. Therefore it is important to develop systems enabling to actively monitor and regulate these factors.

Among the existing technologies to mitigate these risks, various specialized support surfaces have been developed. These include specialized pressure-redistributing mattresses, such as alternating pressure and low-air-loss mattresses [2], [3], which help dynamically distribute pressure across the body. Our research team previously proposed the IntelliPad system [4] to manage both normal and shear stresses at the skin-bed interface, which are significant risk factors in pressure injury development [5]. However, this design lacked temperature monitoring and precise load estimation based on multi-mode actuation. Other pads for normalizing contact pressure distribution have been developed and employ lead screw-driven surface manipulators with integrated force sensitive resistor (FSR) sensors that provide pressure feedback [6]. A recent review on sensor-based pressure injury prevention technologies demonstrated the need for actual data acquisition that enable predictive components using intelligent algorithms [7]. The existing approaches for temperature and humidity monitoring include the use of resistive hydrogels [8] and nanowire-based temperature sensors [9]. Related existing built-in sensors for force estimation and monitoring have also been developed recently. Hyperelastic pressure sensors [10] and a conductive sponge pressure sensor [9] have been developed for pressure-sensing applications. Similar liquid metal-based strain sensors have been used for soft robotic gripper and tactile applications [11]. Commercially available strain gauges and air pressure feedback have been used for robotic surgery applications [12]. However, some of the materials used in these sensors limit their applications to be used in medical settings.

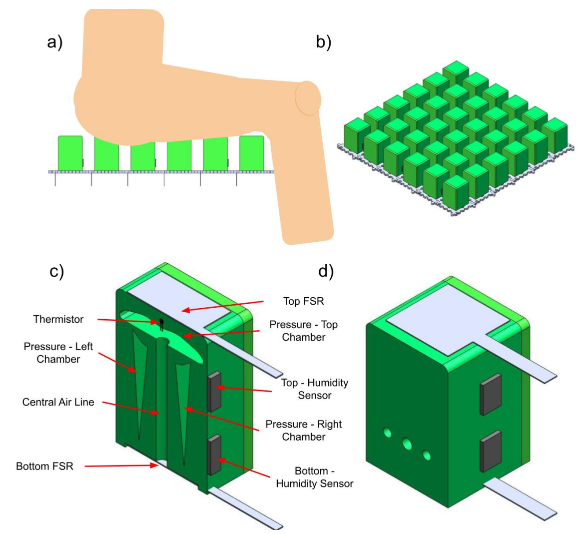

Fig. 1: a) Soft robotic pad setup in a cross sectional view with a user sitting on top. b) View of a full pad. c) A cross-section of the soft actuator with three internal pressure chambers and embedded sensors. d) View of the full actuator. Note that the final configuration only uses the bottom FSR and humidity sensor.

In this paper, we present the design of a soft actuator with embedded temperature, humidity, and force sensors (Fig. 1). The actuator is designed to be integrated into a larger grid and form a soft robotic pad (Fig. Fig. 1b) used as an actively controlled human-pad interface for mitigating risks of pressure injury formation. The design of a proposed actuator was inspired by our previous work [4], [13] and was advanced by the integration of three different sensor modalities. Possible sensor locations were investigated for

This project has been funded by a grant from New Jersey Health Foundation. (M. Trkov).

P. Twomey, V. Varma, and M. Trkov are with the Department of Mechanical Engineering, Rowan University, Glassboro, NJ 08028, USA. (E-mail: twomey33@students.rowan.edu, varmav83@students.rowan.edu, trkov@rowan.edu). (*Corresponding author: M. Trkov*).

each sensor type and the compensation algorithms have been developed to obtain precise estimates. We developed a load estimation algorithm that considers various internal pressures inside the three chambers of the soft actuator in different inflation configurations that affect the reading of the embedded FSRs. Precise load estimation is important for active feedback control of a support surface when multiple actuators are connected to normalize pressure distribution. Additionally, humidity and temperature sensors locations are evaluated and data-driven models are developed to estimate the temperature and humidity at the contact interface. The main contributions of this paper are the developed unique mechatronic platform and algorithms for monitoring factors contributing to pressure injury formation. The developed estimation algorithms can be used for other similar soft robotic applications, where precise monitoring of temperature, moisture, and force is required.

II. Methodology

A. Actuator Design with Embedded Sensors

The dimensions of the soft actuator are 50 mm $\times$ 50 mm $\times$ 80 mm. Actuators are placed in a grid formation with a 25 mm gap (Fig. 1b). Each actuator contains three internal pressure chambers (two side and one top); see Fig. 1c. The fabrication process is demonstrated in Fig. 2. The main body of the actuator has a material hardness of Shore A 22, and is molded from 200 g of dental grade silicone rubber (Elite Double 22, Zhermack, Badia Polesine, Italy), selected specifically due to its inert nature when interfacing with human skin and moisture. The soft actuator integrates a thermistor (10K Ohm, Uxcell, China), an FSR (1.5 inch square, Pololu, Las Vegas, NV), and a humidity/temperature sensor (AHT10, Songhe, China); see Fig. 1. The thermistor and (bottom) FSR are molded into the material, while the humidity sensor and top FSR are attached to the side and top exterior faces of the actuator, respectively. The thermistor is embedded in a silicone rubber layer between the top exterior surface and the top pressure chamber. Three different depths from the top surface were analyzed including 4, 6, and 8 mm deep. The thermistor measures the temperature at the interface of the actuator with the environment (e.g., skin). Two FSR sensors were integrated for testing. One was molded at the bottom and one was attached at the top of the actuator. The top FSR was removed when the temperature tests were performed. Two humidity sensors were attached to the side of the actuator. One was located 10 mm and another 40 mm from the bottom (Fig. 1). These two exterior sensors measure the ambient temperature and humidity.

B. Fabrication of Actuator with Embedded Sensors

Fig. 2 shows the mold setup and fabrication steps. The main body is made from a four-part mold. The mold is designed to create the internal chambers and passageway for the internal wiring and pneumatic lines (Fig. 2a). The side piece is molded separately and attached later (Fig. 2e-h). Four custom molds are first 3D printed using polylactic acid (PLA) material. Two outer ones form the actuator's main shape and an internal one forms the chambers. These molds are first secured together (Fig. 2a). The internal thermistor is temporarily affixed to a desired 4 mm stand-off in the top of the mold with glue. Then the silicone rubber is mixed and poured into the mold (Fig. 2b). The fourth mold that is used as a lid to form the inlets for the air chambers is pressed on top to create the side ports (Fig. 2c). The silicone cures for 90 minutes. The demolding process starts with the removal of a lid and proceeds with removing the bottom shaft mold to reveal the created cavities (Fig. 2d).

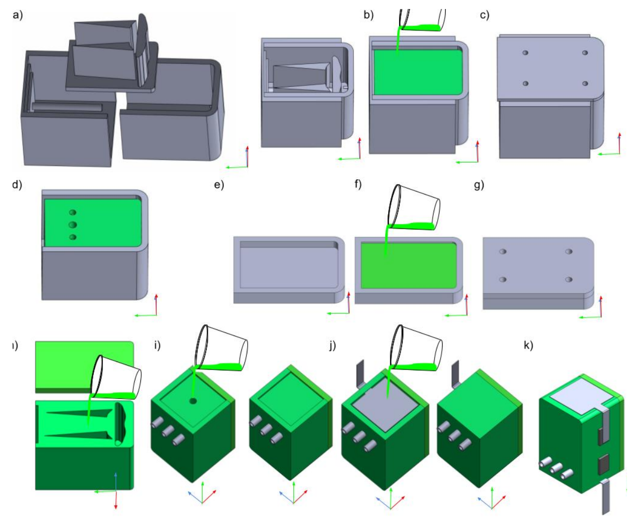

Fig. 2: Fabrication of soft actuator with embedded sensors. a) Preparation of 4-part 3D printed mold. b) Silicone is poured into the mold. c) Mold cap is placed onto mold to make airline pass-through holes. d) After 90 minute curing the actuator is de-molded. e) Preparation of 3D printed mold for actuator sidewall. f) Silicone is poured into mold. g) Placing mold cap onto mold ensuring sidewall has correct thickness. h) Attaching sidewall to actuator's main body. i) Filling in remaining space in central airline after airlines have been run through actuator body. j) Placing FSR in bottom mold cavity and covering it with silicone to seal it. k) Attach FSR and humidity sensors on top of actuator.

Following the demolding of the main body, lead wires for the embedded thermistor and pneumatic line for the top chamber are routed through the body. The lead wires are soldered to the sensor when the mold is still open. An additional mold and a lid are 3D printed to form the sidewall of the actuator. A mold for the sidewall of the actuator (Fig. 2e) is filled with silicone rubber (Fig. 2f) and a lid placed on top. All lids contain holes for the removal of any access material. The prepared sidewall is then attached to the open end of the mold (Fig. 2h) to seal the chambers. The central air-line hole at the bottom part of the actuator is sealed (Fig. 2i), before the FSR is molded inside (Fig. 2j) to produce the final actuator (Fig. 2k). To test the optimal FSR placement, the top FSR and two humidity sensors are attached as shown in Fig. 2k.

C. Determining Optimal Placement of Humidity Sensor

An important factor in preventing pressure injuries is to keep the skin cool and dry [14]. To effectively monitor the micro-climate at the skin-pad contact, our system is designed to estimate the humidity levels at these contact surfaces. This approach is essential because direct measurement of humidity is not feasible as the sensors cannot be in direct contact with the skin due to the electronics in the sensor and rigid sensor housing. Therefore, the estimation is achieved by a humidity sensor placed on the outside surface of the actuator and use a data-driven model utilizing the local humidity in the channels between the actuators. To determine if the distance from the actuation surface had an effect on the sensor reading, we prepared a small grid of actuators and placed two sensors on a single actuator (Fig. 3a).

Fig. 3a shows the experimental setup to test the optimal sensor location. To simulate increasing humidity at the top surface of a grid of four actuators, a microfiber towel was placed over and a spray bottle was used to mist the towel. The towel was sprayed every 15 seconds from a distance of 8 inches above the towel. A control humidity sensor was fixed directly under the towel to serve as a reference. The overall test was run for 35 min to investigate the sensor responses even after the control measurements reached 100% humidity. We examined the humidity measurements by comparing values of both humidity sensors to the control values. To obtain precise estimates, we utilized a data-driven learning approach. With minimal difference between the top and bottom results we identified optimal placement to be the bottom location. The humidity sensor was then used to train a neural network with a structure as shown in Fig. 4a to create a model for accurate humidity estimation based on measurements of a single sensor (see Section II-F).

D. Determining Optimal Placement of Thermistors

One of the factors in preventing the development of pressure injuries in long-term care patients is to prevent the formation of hot spots on the skin [15]. Therefore, our system aims to measure the skin contact temperature by sensing the temperature at the actuator's top surface that will be in contact with the skin. For this purpose, we embedded a thermistor in the top layer of the actuator. To determine the optimal distance of the thermistor from the contact surface, we prepared three samples with a thermistor embedded at depths of 4, 6, and 8 mm. Smaller depths were not considered to avoid possible perforation of the layer.

We investigated thermal conductivity by comparing the thermistor's readings with the measured reference temperature to create a compensation algorithm. To test this, samples were placed on a temperature-controlled surface (i.e., 3D printer's bed) and its accuracy was validated with a non-contact thermometer. A custom G-code for an Ender-3 3D printer was prepared to heat the printer's bed. The testing regime was set to increase in varying temperatures steps of 10°C, 5°C, 2°C, and 1°C and record the response rates at different temperature gradients ΔT. Each test was run individually with the sample located in the center of the bed directly over the heating element. The bed was allowed adequate time between tests to fully cool back to room temperature. The results of the optimal placement were

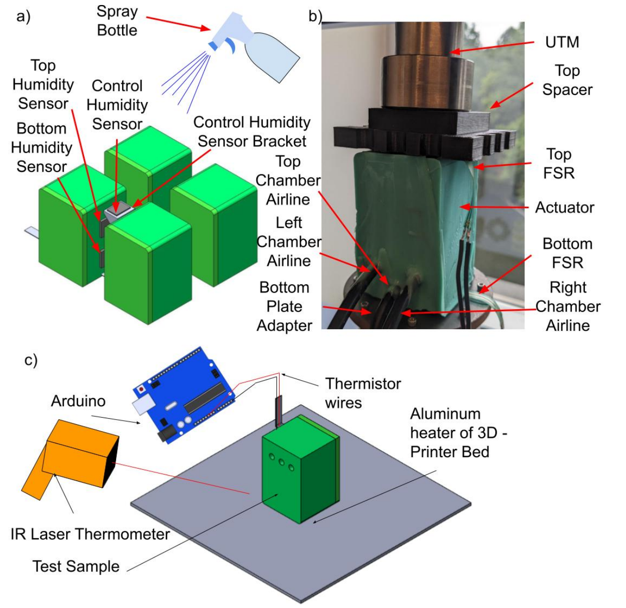

Fig. 3: a) Experimental setup for humidity sensor placement test. A microfiber towel (not shown) was placed over the top and sides of four actuators placed in a grid 25 mm apart. The bottom and top humidity sensors were placed 10 mm and 40 mm from the bottom, respectively. The reference humidity sensor was placed at the top surface touching the microfiber towel. The towel was sprayed every 15 seconds by a spray bottle from a distance of 8 inches. b) The experimental setup for testing optimal placement of FSR sensors. The actuator is placed in a UTM that exerts normal load. c) Experimental setup for thermistor placement test. Samples with the 4, 6, or 8 mm thermistor depth is placed onto the bare heater plate of 3D-printer. G-code with temperature profile is selected to control the bed temperature in set intervals. Bed temperature readout is confirmed with an IR laser thermometer, and the thermistor data is recorded by an Arduino.

utilized to train a neural network (Fig. 4b) to obtain estimates of the contact surface temperature (see Section II-F).

E. Determining Optimal Placement of embedded FSRs

With the goal of normalizing the pressure distribution over the grid array of the soft actuators, optimal placement of FSRs within an individual soft actuator was investigated. The choice of FSR placement holds significance in characterizing its response to the applied forces. We tested two specific locations (i.e., at the top and bottom of the actuator). The experimental setup is shown in Fig. 3b. The actuator was placed in a universal testing machine (UTM) with all ports open (i.e., no applied pressure in chambers). The actuator was compressed vertically for 7.5 mm with a maximum exerted force of 120 N. The FSR values were recorded from a 12-bit Analog-to-Digital converter. Force and displacement readings from the UTM's load cells and values from both FSRs were synchronously collected for comparison purposes.

Due to the fact that the internal pressures in air chambers affect the FSR readings, we experimentally investigated their effects. We performed tests by pressurizing all three chambers in different combinations accounting for every combination resulting in 8 tests in total. To compensate for their effects we designed an estimator utilizing a data-driven learning approach (see Section II-F).

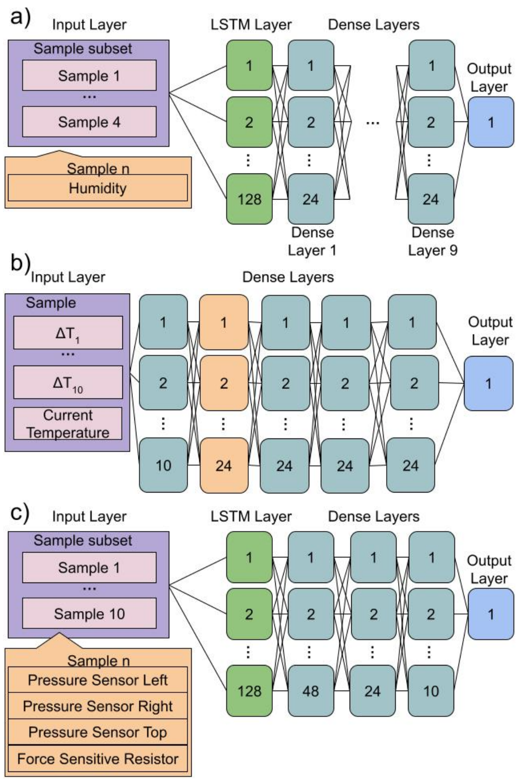

Fig. 4: Network topology of the each of the learning models. a) The Humidity estimation network consists of 10 hidden layers. The first layer consists of 128 LSTM neurons, followed by 9 layers of 24 neurons, and the output, respectively. Each neuron uses a rectified linear activation function. Each input represents a set of 4 humidity samples. b) The temperature estimation network consist of five hidden layers. The size of all layers is 24, except for the input layer, which is 10. The layers shown in blue color use rectified linear activation function, and the one in orange color uses a sigmoid activation function. Each input consists of the current thermistor reading and the temperature difference values (ΔT) for the last 10 time steps. c) The force estimation network consists of 4 hidden layers. The first layer consists of 128 LSTM neurons, followed by a layer of 48 neurons, 24 neurons, 10 neurons, and the output, respectively. Each neuron uses a rectified linear activation function. Each input represents a set of 10 samples with each sample consisting of 4 data points from sensors. The data points are the raw values from the left, right, and top pressure sensors and the raw FSR sensor value.

F. Multi-modal Compensation Matrix Training

To obtain estimates about the exerted normal load, contact temperature, and humidity, we utilize a learning approach by creating neural networks to train a compensation matrix and obtain estimates. The model can capture complex behavior of the non-linear material/structure/environmental responses and compensations due to imperfect sensor location and their readings. We employ a Long Short-Term Memory (LSTM) network stacked with a dense network configuration. An LSTM network, known for its ability to capture sequential dependencies and long-term dependencies in data, offers a dynamic framework for learning and predicting the model's response. We utilize this approach with different network typologies to estimate the humidity (Fig. 4a), contact temperature (Fig. 4b), and normal load under varying inflation conditions (Fig. 4c). All data sets were split into 70% for training and 30% for testing.

The training regime involves feeding the LSTM network with data obtained when loading the samples during UTM testing with different chamber pressurization configurations. The resulting compensation matrix enables accurate normal load predictions regardless of the pattern of chamber pressurization.

The learning process is then performed for temperature estimation considering only one thermistor whose depth was identified as optimal. Our network was designed to consider the rate of change of temperature ΔTs and the current temperature data from the thermistor and correlate them to the surface temperature. Therefore, the input data was formatted to include the current temperature and temperature gradients from the last ten time steps (ΔT_1, ...,ΔT_{10}). Such structured data was fed into the training of a neural network, whose structure is shown in Fig. 4b. Lastly, the learning process for humidity estimation considers only data from the humidity sensor whose height was identified as optimal. The network uses four samples of data from the humidity sensor and correlates them to the control humidity value. Fig. 4a shows the neural network structure.

III. Results

A. Optimal Placement of embedded FSRs

The resistance values of top and bottom FSRs were compared to determine when sensors become saturated. Fig. 5 shows a comparison of their resistance values. During the tests, the top FSR becomes fully saturated at a load of approximately 105 N, while the bottom FSR does not fully saturate (up to 120 N). Despite the smaller value range of the bottom FSR, both resistances intersect at approximately 45 N. This yields a similar window for the high-end force range resolution and reduced resolution for the lower range on the bottom FSR. However, due to the average pressure at the human buttock and cushion interface being 20 kPa [16], the higher range is important and the bottom FSR was chosen as the preferred location.

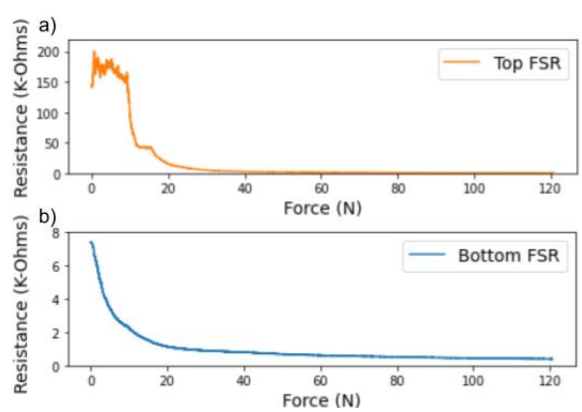

Fig. 5: Average experimental FSR resistance for load applied on the non-pressurized actuator.

B. Optimal Placement of Humidity Sensors

Fig. 6 shows the results of humidity measurements for both humidity sensors. The measurements are compared to the true/control values. Sensors at both locations show almost identical measurements. Therefore, the location of the bottom sensor was chosen as optimal to minimize possible physical interference when actuators are displaced horizontally. Estimation results of a trained model show convergence of the model to the actual values (Fig. 6). The model can capture rapid changes in humidity, while its ability to predict humidity saturation is achieved with a delay (6 min). Despite the delay, the estimates show significant improvement compared to the raw humidity reading of the sensor where the sensor only reaches 81% humidity, which would result in an error of 19%.

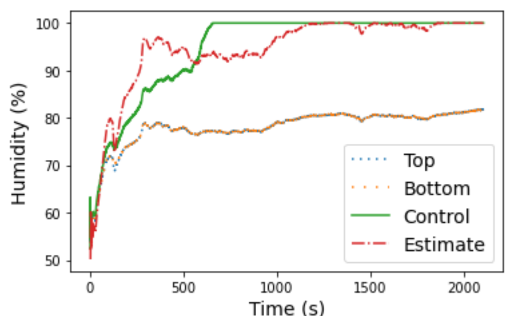

Fig. 6: Comparison results for the relative humidity measurements of each sensor. Results are compared to the control/reference value and filtered predicted values of our learning model.

C. Optimal Placement of Embedded Thermistors

Fig. 7 shows the results of thermistor measurements at three different locations. The sensor located at a depth of 4 mm showed the best performance and was chosen as the optimal location of a sensor due to the reduced thermal lag. The temperature steps show calibration for when a patient may first get on the pad, and shows the ability to adjust to smaller temperature changes. The data from this sensor was used to train the neural network model to obtain the estimates. Fig. 7 shows the comparison of estimates to the true (bed) temperature. The model is able to estimate the surface temperature for both large and small temperature changes well. This helps to reduce faulty readings due to the delayed heat conduction through the material.

D. Multi-modal Learning Model for Load Estimation

Fig. 8 shows the normal load estimation results for various patterns of internal pressures (15 psi) in the air chambers as they affect the FSR readings. The estimation results match the true values measured by the UTM load cell. In the high load regions, the estimates show increased deviation from the expected true value compared to low force values. This might be due to the sensor reaching near its saturation point. The model slightly under-predicts values when the top and one side chambers are simultaneously inflated (Fig. 8e-f). This might be due to modified stability of the actuator's structure, due to bending of the internal walls and therefore, uneven

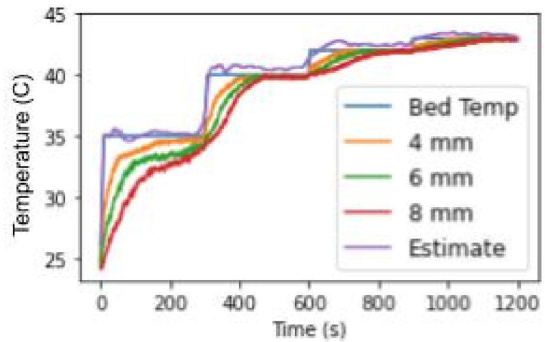

Fig. 7: Comparison of temperature readings for sensors at depth of 4, 6, and 8 mm from the top surface of the actuator along with the true values (controlled bed temperature) and filtered estimated values of our learning model for sensor depth of 4 mm.

load on the FSR sensor. Nevertheless, results show that the trained model can reasonably predict normal load for any given pattern of internal pressure conditions. The model is able to predict with minimal error for each loading condition as shown in Fig. 8.

E. Discussion

To improve resolution of high range results of the FSR sensors, future iterations may implement a 16-bit analog-to-digital converter (ADC) to capture smaller changes in resistance The bottom FSR is also ideal due to the initial irregularity in resistance readings of the top FSR when initially loaded (Fig. 5). This irregularity may be due to the increase in errors that occur when the sensor is bent [17]. Due to a soft mounting surface, the top FSR is bound to bend during the deformation of the actuator. The bottom FSR placement is also preferred due to practical reasons, including easier maintenance and cleaning of the sensors when used by the patients, easier integration of the sensors as there is no direct contact with the skin, and better thermal conductivity that does not affect readings of the embedded thermistor. The bottom humidity sensor location was selected as ideal due to the minimal effect of the distance between the top and bottom locations. Having the sensor further away from the top of the actuator reduces the chance of direct skin contact that can cause irritation, and allows for easier maintenance and cleaning of the pads. Lastly the 4 mm thermistor depth was selected for its quickest response times. We acknowledge that our setup has not been tested with a human sitting on it to investigate the coupling affect of sensors or in a clinical setting and these testings remain part of our future plans.

IV. Conclusion

In this paper, we presented the integration of embedded temperature, humidity, and FSR sensors in a soft robotic actuator, and investigated their possible locations. In addition, we trained data-driven models to estimate the force, humidity, and temperatures under various loading and environmental conditions. The normal load estimator can accurately account for the various chamber pressurization configurations that alter the stiffness of the actuator. Our

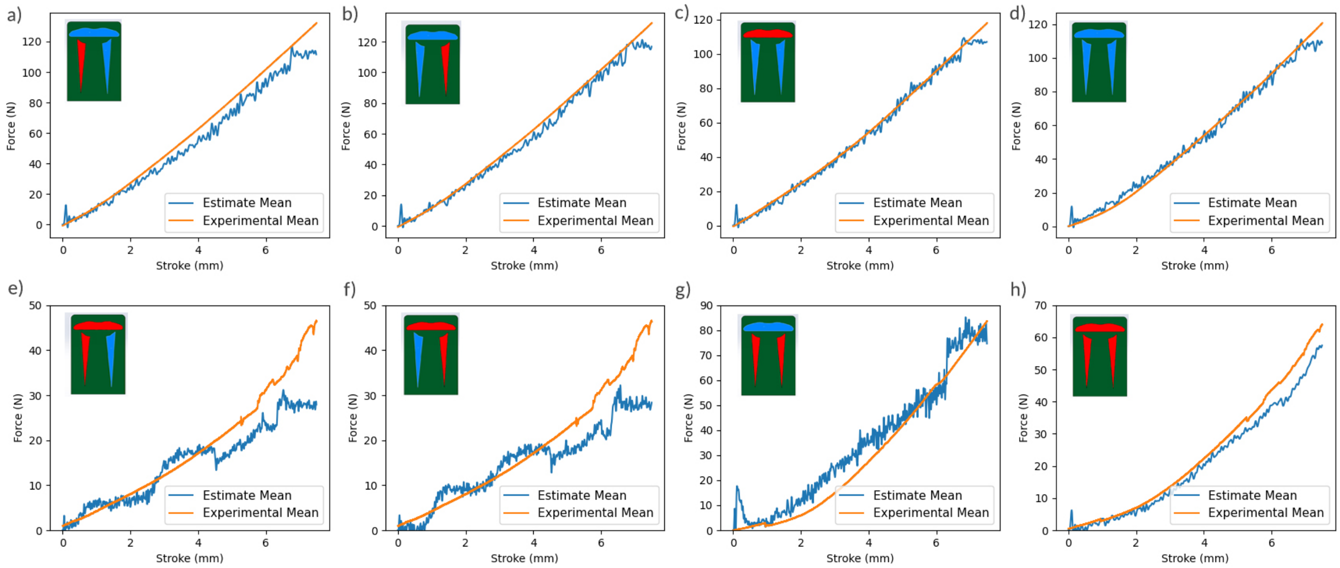

Fig. 8: Results of load predictions from the model are compared to the average true-load on the actuator. Combination of inflated chamber to 15 psi are shown for a) left only, b) right only, c) top only, d) none inflated, e) left and top, f) top and right, g) left and right, and h) all chambers. Chambers marked in red color were pressurized, while those in blue were not.

models can estimate humidity and temperature at the contact surface. The process of adding these sensors into the fabrication process allows for feedback from the contact interface and adaptation of conditions to patient needs. This model enables estimation of the true load accounting for the variable stiffness of the actuator. This feature enables the utilization of the actuator in a grid format, for normalizing the pressure applied to patients. Future work will include more testing configurations with the addition of testing chambers under vacuum. This preliminary work enables the development of testing actuators in a full grid configuration with a human thigh-buttock physical analogue developed in [18] to further validate the model.

References

[1] C. Russo, C. Steiner, and W. Spector, *Hospitalizations Related to Pressure Ulcers Among Adults 18 Years and Older, 2006: Statistical Brief# 64*, 12 2008.

[2] C. Shi, J. C. Dumville, N. Cullum, S. Rhodes, A. Jammali-Blasi, and E. McInnes, “Alternating pressure (active) air surfaces for preventing pressure ulcers,” *Cochrane Database of Systematic Reviews*, no. 5, 2021. [Online]. Available: https://doi.org//10.1002/14651858.CD013620.pub2

[3] B. Serraes, A. Hecke, H. Van Tiggelen, C. Anrys, S. Verhaeghe, and D. Beeckman, “An exploration of nursing home residents’ experiences of a non-powered static air mattress overlay to prevent pressure ulcers,” *International Wound Journal*, 06 2020.

[4] M. Raeisinezhad, N. Pagliocca, B. Koohbor, and M. Trkov, “Intellipad: intelligent soft robotic pad for pressure injury prevention,” in *2020 IEEE/ASME International Conference on Advanced Intelligent Mechatronics (AIM)*. IEEE, 2020, pp. 685–690.

[5] P. Joyce, Z. Moore, and J. Christie, “Organisation of health services for preventing and treating pressure ulcers,” *Cochrane Database of Systematic Reviews*, vol. 2018, 12 2018.

[6] R. Yousefi, S. Ostadabbas, M. Faezipour, M. Nourani, V. Ng, L. Tamil, A. Bowling, D. Behan, and M. Pompeo, “A smart bed platform for monitoring & ulcer prevention,” in *2011 4th international conference on biomedical engineering and informatics (BMEI)*, vol. 3. IEEE, 2011, pp. 1362–1366.

[7] A. Silva, J. Metrôlho, F. Ribeiro, F. Fidalgo, O. Santos, and R. Dionisio, “A review of intelligent sensor-based systems for pressure ulcer prevention,” *Computers*, vol. 11, no. 1, 2022. [Online]. Available: https://www.mdpi.com/2073-431X/11/1/6

[8] Z. Lei and P. Wu, “A highly transparent and ultra-stretchable conductor with stable conductivity during large deformation,” *Nature communications*, vol. 10, no. 1, p. 3429, 2019.

[9] W. Yang, M. Xie, X. Zhang, X. Sun, C. Zhou, Y. Chang, H. Zhang, and X. Duan, “Multifunctional soft robotic finger based on a nanoscale flexible temperature–pressure tactile sensor for material recognition,” *ACS Applied Materials & Interfaces*, vol. 13, no. 46, pp. 55 756–55 765, 2021.

[10] Y.-L. Park, C. Majidi, R. Kramer, P. Berard, and R. Wood, “Hyperelastic pressure sensing with a liquid-embedded elastomer,” *Journal of Micromechanics and Microengineering*, vol. 20, 12 2010.

[11] R. A. Bilodeau, E. L. White, and R. K. Kramer, “Monolithic fabrication of sensors and actuators in a soft robotic gripper,” in *2015 IEEE/RSJ International Conference on Intelligent Robots and Systems (IROS)*. IEEE, 2015, pp. 2324–2329.

[12] T. Takizawa, T. Kanno, R. Miyazaki, K. Tadano, and K. Kawashima, “Grasping force estimation in robotic forceps using a soft pneumatic actuator with a built-in sensor,” *Sensors and Actuators A: Physical*, vol. 271, pp. 124–130, 2018.

[13] M. Raeisinezhad, N. Pagliocca, B. Koohbor, and M. Trkov, “Design optimization of a pneumatic soft robotic actuator using model-based optimization and deep reinforcement learning,” *Frontiers in Robotics and AI*, vol. 8, 2021. [Online]. Available: https://www.frontiersin.org/articles/10.3389/frobt.2021.639102

[14] J. Kottner, J. Cuddigan, K. Carville, K. Balzer, D. Berlowitz, S. Law, M. Litchford, P. Mitchell, Z. Moore, J. Pittman *et al.*, “Prevention and treatment of pressure ulcers/injuries: The protocol for the second update of the international clinical practice guideline 2019,” *Journal of tissue viability*, vol. 28, no. 2, pp. 51–58, 2019.

[15] T. Bui, P. Lestriez, D. Pradon, K. Debray, and R. Taiar, “The prevention of pressure ulcers: biomechanical modelization and simulation of human seat cushion contributions,” in *Proceedings of the International Conference on Advances in Computational Mechanics 2017: ACOME 2017, 2 to 4 August 2017, Phu Quoc Island, Vietnam*. Springer, 2018, pp. 1157–1170.

[16] M. Grujicic, B. Pandurangan, G. Arakere, W. Bell, T. He, and X. Xie, “Seat-cushion and soft-tissue material modeling and a finite element investigation of the seating comfort for passenger-vehicle occupants,” *Materials and Design*, vol. 30, no. 10, pp. 4273–4285, 2009.

[17] C. Ahmadizadeh and C. Menon, “Investigation of regression methods for reduction of errors caused by bending of fsr-based pressure sensing systems used for prosthetic applications,” *Sensors*, vol. 19, no. 24, 2019.

[18] P. Twomey, Z. Bravo, and M. Trkov, “Mechatronic design of a thigh-buttock analogue and instrumented soft pad for pressure injury prevention,” in *Proc. of 2024 IEEE/ASME International Conference on Advanced Intelligent Mechatronics (AIM)*, Boston, MA, July 2024.